Modelling and Control of a 50kW SiC-based Isolated DAB Converter for Off-Board Chargers of Electric Vehicles

Haaris Rasool[1,2], Manh Tuan Tran[1,2], Sajib Chakraborty[1,2], (Member, IEEE), Joeri Van Mierlo[1,2], (Senior Member, IEEE) Thomas Geury[1,2], (Member, IEEE), Mohamed El Baghdadi[1,2], (Member, IEEE) and Omar Hegazy[1,2], (Senior Member, IEEE)

[1]MOBI-EPOWERS Research Group, ETEC Department, Vrije Universiteit Brussel (VUB), Pleinlaan 2,1050 Brussels, Belgium
[2]Flanders Make, 3001 Heverlee, Belgium

*Corresponding author: Omar Hegazy (omar.hegazy@vub.be).

Keywords

«Bi-directional», «Charging infrastructure for EVs », «Wide bandgap», «Power flow control»,

Abstract

The paper proposes the design of a 50kW isolated DC-DC Dual Active Bridge (DAB) converter for a high-power off-board charger for Electric vehicles (EVs) applications. The detailed electro-thermal simulation of the wide band gap (WBG) (i.e., SiC MOSFETs)-based bidirectional DAB is performed to determine the performance of the system in terms of efficiency at high-power operation. A linear model based on system identification has been created to design the control approach accurately. Dual-loop phase shift constant-current (CC) and constant-voltage (CV) control strategy is implemented on the dynamic simulation model at a higher switching frequency to validate the stability of the designed controller. The proposed DAB operates with an acceptable ripple and dual-loop voltage-current control that comprehensively tracks reference commands, while the maximum efficiency achieved is approximately 97.5% at rated power.

1. Introduction

With increasing awareness of climate change, research efforts are focusing on decarbonizing vehicle emissions. The automotive and energy sector are focusing on battery electric vehicles (BEVs) and renewable energy resources (RERs). Therefore, this also involves new challenges such as an increasing energy demand by charging BEVs and grid stability issues because of the intermittent nature of RERs. However, today it is necessary to develop appropriate BEV chargers that allow bidirectional power flow and intelligent strategies to manage the charging process [1].

There are two types of charging systems for EVs: conductive charging and inductive charging. Conductive charging systems are better established than inductive charging, which is widely accepted in electrified transport. In conductive charging, the vehicle stays in direct contact with the supply through the socket to transfer power. Conductive charging is further classified into on-board and off-board charging systems [2]. The Society of Automotive Engineers (SAE) and Electric Power Research Institute (EPRI) have categorized EV charging levels as level-1, level-2, level-3, and next-generation ultra-fast charging. The level-1 and level-2 chargers are considered on-board chargers to inject power in batteries. However, a level-3 charger typically works as an external converter and can effectively manage high power flow. Fast DC charger is associated with level-3 and next-generation charging [3], [4]. The off-board charger reduces on-board circuitry to reduce the overall weight of the vehicle [5]. During inductive charging, there is no physical contact with the supply to transfer power to the vehicle. The wireless charging technique utilizes an electromagnetic field to transfer power.

The low-frequency or high-frequency transformer provides galvanic isolation between the EV and the grid. The filter is used to eliminate unwanted harmonic currents. Power Electronic Converters (PECs) convert the three-phase AC power from the grid into DC power used to charge the EV battery. The control unit operates the switches of PEC to adjust the voltage and current level, which the BEV can accept. Since the charger is characterized by high voltages and currents, galvanic isolation between the electrical grid and the BEV is required to ensure a safe operation. This can be realized by two transformer topologies: a low-frequency transformer (LFT) or a high-frequency transformer (HFT). Typically, the

topology with an isolated DC-DC converter with HFT is considered for high power Off-board charger design (i.e., 50 kW and beyond). It comprises converting incoming AC power to a fixed DC output using an Active Front End (AFE) converter, which is then converted to the demanded voltage of the EV using an isolated DC-DC converter. This topology contains an LCL filter, an AC/DC bidirectional converter, a DC filter, an isolated DC-DC bidirectional converter with a high frequency (HF) transformer and a DC link filter [6], as shown in Fig. 1. The bidirectional off-board charger connects to the battery pack of EVs, which later supplies the inverter and drives the electric motor. The battery pack is also connected with a buck DC-DC converter inside the vehicle, which provides the auxiliary power supply of EVs.

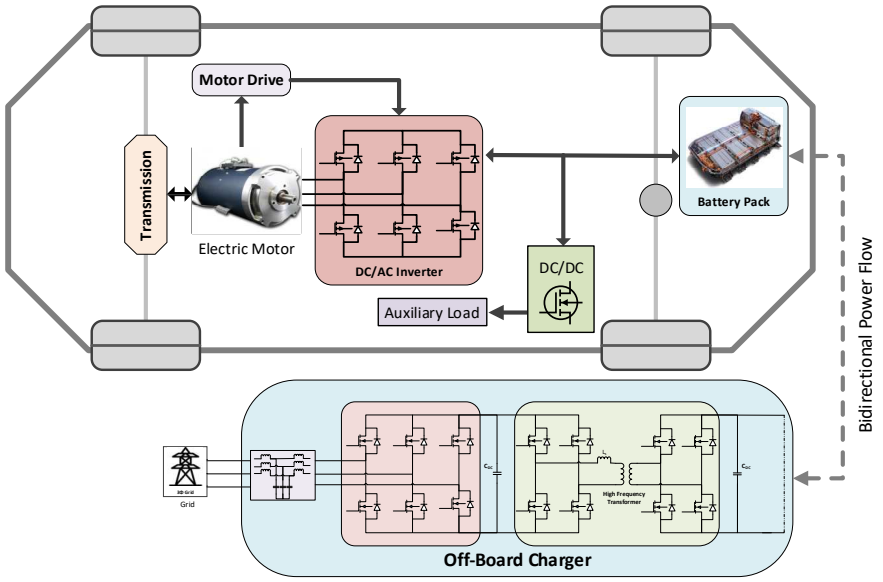

Fig 1. Off-Board charging arrangement for fast DC charging of BEVs.

The different topologies of isolated DC-DC converters are discussed in the literature, such as full-bridge LLC converter (FBLLC), phase-shifted full-bridge converter (PSFB) and dual active bridge (DAB) converter. The DAB converter is best suited for high voltage applications for bidirectional power flow thanks to its higher efficiency, soft switching commutation capabilities and a reduced number of devices [7]. The modularity and synchronization structure in DAB topologies, allows converters to achieve higher output power and facilitates the two-way operation of power flow for battery charging (G2V) and discharging (V2G) applications. Therefore, DAB topology is beneficial where the following factors are required: galvanic isolation, power density, high voltage conversion ratio and reliability [7], [8]. These factors make an ideal charging station and energy storage system. Thus, this paper proposes a DAB DC-DC converter to design a 50 kW off-board charger for BEVs. Furthermore, the stepwise design methodology and control design of the DAB converter is analyzed in this paper. The aim of this study is to integrate the WBG SiC semiconductor and high-switching frequency control approach for the emerging application of off-board chargers. At the same time, this paper depicts the design of an isolated bidirectional DC-DC converter for an off-board fast charger. The converter provides isolation between the grid and the battery of the EV. The objective of designing an isolated DC-DC converter is to get higher efficiency and high specific power by eliminating the classical low-frequency grid-side transformer. The conventional battery charging technique is known as constant current-constant voltage (CC-CV) mode. The idea is that the battery is charged with maximum constant current according to the battery cell capacity up to cut-off voltage and then charged at constant voltage until the drawn current decreases to C/10 or less, where C states the charge or discharge rate of the battery over one hour [4]-[5]. The proposed control approach allows batteries to be charged in different modes based on different voltages and current levels to keep the battery life maximal [9].

This paper is arranged into different sections. Section 2 of this paper describes the system and control architecture. Section 3 illustrates the design methodology of the DAB converter. In Section 4, the detailed loss modelling of DAB converter in a dynamic simulation model is explained. Section 5 is dedicated to

control design, whereas Section 6 describes the simulation results. Finally, the conclusions are provided in Section 7.

2. System and control architecture

In this paper, an isolated DAB DC-DC converter is designed and simulated. It consists of a primary side capacitor, coupling inductor, high-frequency transformer, and secondary side capacitor. The SiC-based power modules are utilized to design and operate at a high switching frequency. A controller is required to drive eight switches of the DAB converter and regulate the power according to the requirement of the battery capacity. The topology and bi-directional control architecture of the DAB converter is illustrated in Fig. 2.

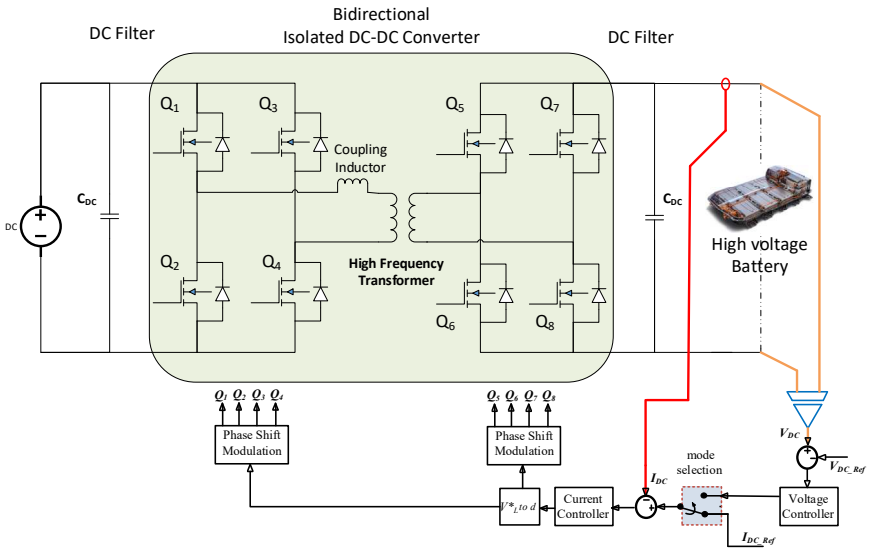

Fig 2. Isolated DAB DC-DC converter and control architecture.

3. DAB Phase Shift and Inductor Selection

The phase shift of the converter is dependent on the value of the inductor L of primary side of the DAB converter. In this paper, the turns ratio of the transformer considered, n, is 1 and the switching frequency f_s is 40kHz. The required total leakage inductance is calculated from Eq. 1, 2, and Fig. 3 (a) [7]-[8]. It is approximately 36 µH at a phase shift of 60° for the 50kW power. The planar transformer's primary side leakage inductance measured in the lab is 4µH. The coupling inductor of 32 µH is introduced on the primary side of the DAB converter with a combination of the leakage inductor of the transformer. Therefore, a total inductor of 36µH is required to achieve the desired power transfer with phase shift control.

$$\phi = \frac{\pi}{2}\left(1 - \sqrt{1 - 8\frac{nf_S L P_{out}}{V_{in}V_{out}}}\right) \tag{1}$$

where,

$$n = \frac{V_{out}}{V_{in}} \tag{2}$$

Another analysis is performed between the output power and phase shift ϕ, to analyze the maximum allowable power of DAB DC-DC converter with a phase shift. In this investigation, all other parameters are considered constant in Eq. 3, such as turns ratio n is 1, inductance L is 36µH, and the switching frequency f_s is 40kHz. The plot of Fig. 3 (b) shows that the peak power is transferred when the phase shift is 90°. This analysis is very important to check the power safety margin while designing a converter at a given power rating. This analysis shows that, maximum rated power can be delivered without any interruption at phase shift of 60°. The sinusoidal curve of the power versus phase shift illustrates the flow of power in bidirectional mode such as V2G and G2V for the off-board charger. The limit in phase shift will be applied for the closed loop control implementation in order to limit the power of the converter.

$$P_{out} = \frac{V_{in}V_{out}\phi\left(1-\left|\frac{\phi}{\pi}\right|\right)}{2\pi f_s n L} \tag{3}$$

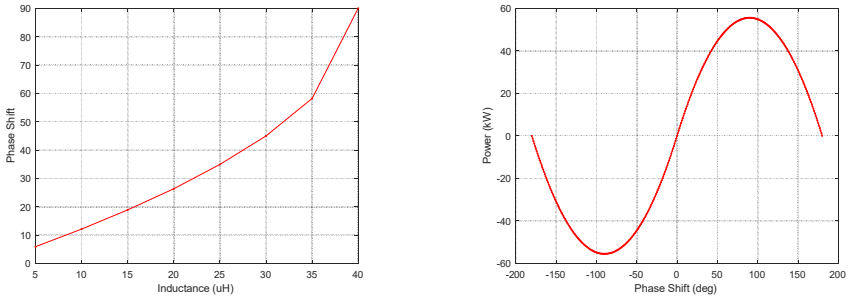

(a) (b)

Fig 3. Inductor selection: (a) Phase shift vs inductance, (b) power versus phase shift.

4. DAB Power Loss Modelling

In this paper, the power loss model of the DAB converter is developed in simulation to predict the overall efficiency. The power loss model includes half-bridge (CAS300M17BM2) module loss, high-frequency transformer loss and passive components loss.

4.1 Converter Loss Model

A. Conduction Power Losses

The conduction power losses of the power electronic converter depend on the voltage-current characteristic of the transistor and the diode. It can be calculated using Eqs. (4-6) [10]–[12]. V_{ds}[V] and i_d [A] of Eq. 4, represent the forward saturation voltage and drain current of the MOSFET. V_{ds} is obtained as a function of i_d and the junction temperature. It can be estimated by using an interpolation technique on the datasheet characteristics of the half-bridge module. Integrating the instantaneous power losses over a switching cycle T_{sw} (sec) gives an average value of the MOSFET conduction losses as in Eq. (4).

$$P_{CM} = \frac{1}{T_{sw}} \int_0^{T_{sw}} P_{cond_{loss}}(t)dt = \frac{1}{T_{sw}} \int_0^{T_{sw}} V_{ds}(t) i_d(t)\, dt \tag{4}$$

The conduction loss of the body diode is calculated using Eq. (5).

V_f (V) and i_f (A) represent the forward saturation voltage and current of the diode, respectively. V_f is a function of the junction temperature and the current i_f.

$$P_{CD} = \frac{1}{T_{sw}} \int_0^{T_{sw}} P_{D\ cond_{loss}}(t)dt = \frac{1}{T_{sw}} \int_0^{T_{sw}} V_f(t) i_f(t)dt \tag{5}$$

The total conduction loss is calculated by adding up the average power losses of the MOSFET and the diode, as represented in Eq. (6).

$$P_{total_C} = P_{CM} + P_{CD} \tag{6}$$

B. Switching Power Losses:

The estimation of the switching losses in the device is done by using datasheet characteristics. A complex strategy with a small step size is needed to estimate the losses that occur during the device's turn-on and turn-off transients. However, a lookup table method is more feasible and easier to implement for estimating the switching power losses. The switching energies E_{swon} (mJ) and E_{swoff} (mJ) are used to estimate the switching power loss as expressed in Eq. (7). The switching energies of MOSFETs are defined as functions of drain current, junction temperature and drain voltage [13]–[16].

$$E_{total} = E_{sw_{on}} + E_{sw_{off}} \tag{7}$$

Hence, the switching power losses can be estimated from the energy losses expressed in Eq. (8).

$$P_{Msw_{loss}} = \left(E_{sw_{on}} + E_{sw_{off}}\right).f_S \tag{8}$$

where, f_S is the operating switching frequency.

The switching losses for a diode are defined by the reverse recovery characteristics but can also be calculated from the reverse recovery charge and reverse recovery time. However, for SiC technology-based MOFET, the switching losses of the diode are negligible. It can be calculated using the relation expressed in Eq. (9), which is dependent on E_{rr}.

$$P_{Dsw_{loss}} = E_{rr} f_S \tag{9}$$

The total average power losses of the MOSFET and body diode can be computed with Eq. (10).

$$P_{total_{sw}} = P_{Dsw_{loss}} + P_{Msw_{loss}} \quad (10)$$

4.2 Transformer Loss Model

Transformers and inductors impact the size and weight of isolated DC-DC converter designs. Increasing the operating frequency reduces the requirement for passive filters. However, increasing the switching frequency beyond a certain value increases the power loss and reduces the efficiency, because of the skin effect and proximity effect. More interleaving can be achieved with a planar transformer to reduce the effect of proximity. The planar transformers have some advantages over conventional transformers and are therefore used in this research. The power density of planar magnets is high. It allows more interleaving, further reducing the conductor losses. Tight control is possible through planar magnets. The compact size of the transformer can support the integration of an additional leakage or coupling inductor with the transformer without the need for a separate component on the board [7][8]. The planar transformer is chosen for the isolated 50kW DAB DC-DC converter design. The manufacturer specification of the high-frequency transformer is depicted in table-I. These parameters are used in simulation design and power loss modelling of a transformer.

Table I: High-frequency transformer specification.

Parameters	Values	Parameters	Values
Power (kW)	50	Turns Ratio Primary to Secondary	10:10
Operating Frequency (kHz)	10-70	Cooling Type	Liquid cold plate
Primary Inductance (mH)	2.3	Estimated Power Loss Core (W)	101 (R_{ac} = 0.0125Ω)
Leakage inductance (μH)	4	Estimated Power Loss Winding (W)	108 (R_{dc} = 0.0133Ω)
Input Voltage (V)	550-900	Estimated Maximum Temperature Rise (°C)	80
Output Voltage (V)	550-900	Length x Width x Height (mm)	293 x 204.5 x 75

4.3 Passive Component Loss Model

The passive filters power loss significantly contributes to the converter design's efficiency. Therefore, the power loss of the inductor and capacitor are calculated using mathematical equations [10].

A. Inductor Losses Calculation

The inductor's total losses depend on the windings and core power losses. It can be determined by Eq. (11).

$$P_{ind_{Total\ loss}} = P_{ind_{loss}} + P_{ind_{core}} \quad (11)$$

The power losses in the inductor windings are represented in Eq. (12).

$$P_{ind_{loss}} = I_L^2 R_{LDC} + \Delta I_L^2 R_{LAC} \quad (12)$$

where I_L (A) is the inductor current, ΔI_L (A) is the inductor current ripple, R_{LDC} (mΩ) is the inductor resistance and R_{LAC} (mΩ) is the AC winding resistance due to the skin effect. R_{LDC} is quantified by Pouillet's law as shown in Eq. (13).

$$R_{LDC} = \frac{\rho N l_T}{A_w} \quad (13)$$

where, ρ (mm.Ω) is the wire resistivity, N is the number of turns, l_T [mm] is the length of the turn and the cross-sectional area of the wire is denoted by A_w (mm^2). The wire for the inductor core can be selected, according to A_w and by the current passing through the inductor.

R_{LAC} can be calculated based on the skin depth S_d [mm] and F_R is the winding resistance ratio [10], as expressed in Eq. (14). Skin depth can also be used for the selection of Litz wire with strand size not bigger than three times the skin depth.

$$R_{LAC} = R_{LDC} F_R \quad (14)$$

Another factor on which the total inductor losses are the core losses, represented by Eq. (15).

$$P_{ind_{core}} = k f_s \left(\frac{2}{\pi^2} 4 f_S\right)^{\alpha-1} B_{pk}^{\beta} V_{core} \quad (15)$$

where k, α, β are the Steinmetz parameters and V_{core} (L) is the volume of the core, which can be extracted from the datasheet of the inductor core material. B_{pk} is the peak magnetic flux density.

B. Capacitor Losses Calculation:

The equivalent series resistance (ESR (mΩ)) of the capacitor is an important parameter to estimate the power loss. The ESR is normally mentioned in the datasheet of the capacitor. The power loss of the capacitor is calculated using Eq. (16) [17].

$$P_C = I_{CRMS}^2 ESR\ (f_S) + I_{leak} V_C \tag{16}$$

where, I_{CRMS} (A) is the RMS current passing through the capacitor, V_C (V) is the average capacitor voltage and I_{leak} (A) is the leakage current passing through the capacitor.

4.4 Efficiency Estimation

System efficiency is a very important variant for the observation of the overall performance of the system. In this paper, the efficiency of an isolated DAB DC-DC converter is estimated using the complete power losses, such as power losses of the SiC MOSFETs, losses in the passive filters and high-frequency transformer loss. The loss of a high-frequency transformer is mentioned in the manufacturer's specifications. The efficiency in percentage is calculated using the DC output power and the total average power losses of the converter according to Eq. (17).

$$\eta = \frac{P_{DC}}{P_{DC} + P_{loss\_MOSFET} + P_{loss_{psve}} + P_{loss\,TR}} 100\ (\%) \tag{17}$$

5. DAB Converter Control Design

This paper proposes dual-loop control for the DAB converter. The PI controllers are tuned to obtain the desired response in terms of overshoot, rise time, and settling time, and tested in a dynamic simulation. All sensors' delays are included in the control system design process. The design and tuning of the controllers have been carried out using gain margin (*gM*) at gain margin frequency (*ωcg*) and phase margin (PM) at crossover frequency (*ωcp*). The block diagram of dual-loop voltage and current control of the DAB DC-DC converter are shown in Fig. 4. It consists of an outer loop constant voltage control, regulating the output voltage in CV mode, and an internal control loop is constant current control, regulating the output current in CC mode. The output of the voltage controller is the reference signal of current controller. The output control signal of current controller is the phase delay, it can be transformed into time delay (i.e., 60° phase delay = $\frac{60^o}{360^o f_S}$ sec time delay). Since the charge control begins with constant current mode, the delay should be limited to 60° to avoid overcharging current. The time delay impacts the delay of the triangular carrier wave for the generation of 50% duty cycle PWM digital signals.

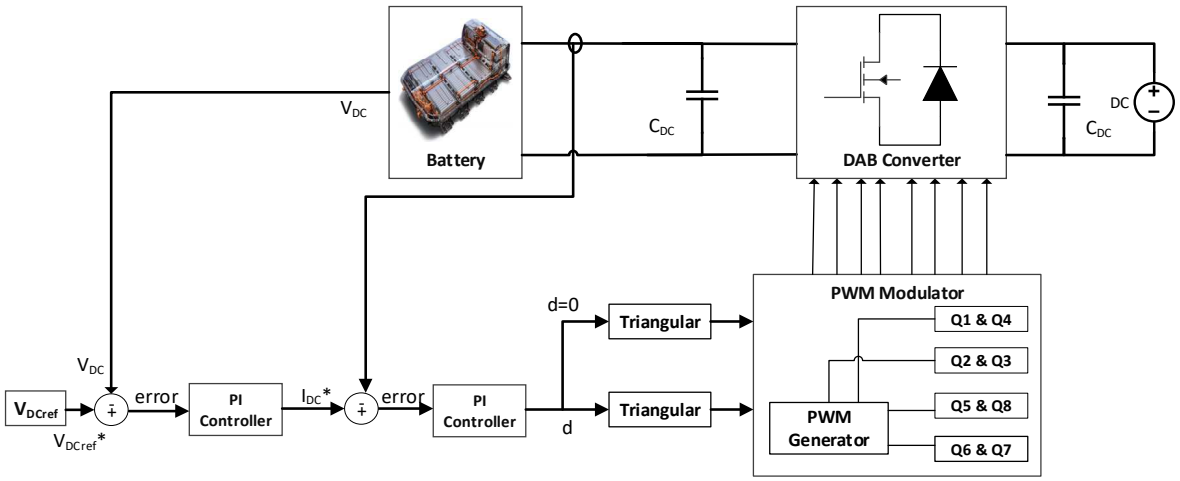

Fig. 4: Dual loop control block diagram of DAB converter.

The closed loop constant current control is designed with the linear model of current $G_{CC_{plant}}$. The transfer function of load current is given in Eq. 18, the input is phase delay and output is load DC current. This second-order transfer function of load current is identified using MATLAB system identification tool (ident). For the system identification, input and output data are logged from the dynamic open-loop

simulation model of DAB DC-DC converter. The input and output is further applied for the identification of transfer function using MATLAB tool. The best match is achieved at 99% with the second-order transfer function $G_{CC_{plant}}$.

$$G_{CC_{plant}} = \frac{I_{DC}}{delay} = \frac{647.7s+2.098\times10^6}{s^2+4011s+2.533\times10^6} \quad (18)$$

The constant current control loop is designed at a crossover frequency of 4kHz with sufficient phase margin, overshoot, rise time, and settling time to ensure fast dynamics in the charging process. The dual loop constant voltage control loop is shown in Fig. 5. The voltage control is designed using the transfer function of DC converter current, output capacitance and maximum load. The transfer function of load DC voltage $G_{VV_{plant}}$ is given in Eq. 19, the input is DC reference voltage and output is load DC voltage.

$$G_{VV_{plant}} = \frac{V_{DC}}{I_{DC_{Ref}}} = \frac{\left(k_p+\frac{k_i}{s}\right)G_{CC_{plant}}}{\left(k_p+\frac{k_i}{s}\right)G_{CC_{plant}}+1} \times \frac{\frac{1}{sC_{DC}}}{\frac{1}{sC_{DC}}+\frac{1}{R_O}} \quad (19)$$

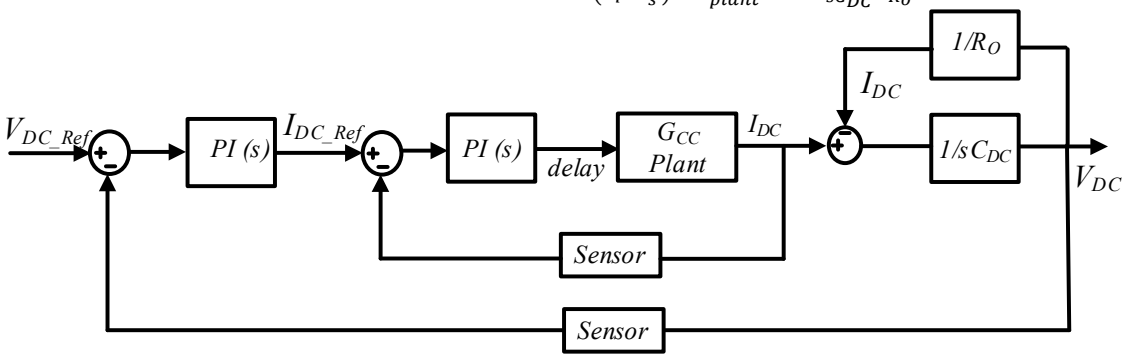

Fig. 5: Voltage loop control of DAB converter.

The closed-loop control design includes the sensors and PWM delays, i.e., 10µs for voltage sensor (LEM DVC 1000-P) delay, 3µs for current sensor (ISB-425-A-802) and 0.5µs for PWM. After close-loop analysis, the PI controllers are tuned according to margins and frequencies. The outer constant voltage control is designed at 50Hz. The inner loop current PI controllers are designed at <1/10 of the switching frequency, which is <4kHz. The control parameters, close loop overshoot, *gM*, *ωcg*, *PM* and *ωcp* of voltage and current control are displayed in Table II. The discrete controller will be implemented in the real-time FPGA platform of dSPACE MicrolabBox.

Table II: Controller design parameters

Controller	Control Parameters	Overshoot (%)	GM (dB)	PM (deg)	Wcp (rad/sec)	Wcg (rad/sec)
Current Control	K_p=37.1, K_i=91453.4	4.6	39.7	86	2.41×10^4	8.14×10^4
Voltage Control	K_p=0.22, K_i=27.4	6	22.1	62	326	1.8×10^3

6. Simulation Results

A dynamics simulation model of the DAB DC-DC converter is established in MATLAB/Simulink. The dual loop voltage-current control strategy is designed and implemented in simulation using specifications at rated power.

6.1 Specification

The specification of DAB DC-DC converter is shown in Table-III. These parameters are used for simulation design and performance validation.

Table III: Simulation design parameters

Parameters	Values
Power (kW)	50
Operating frequency (kHz)	40

Input voltage (V)	700-800
Output voltage (V)	700-800
Half-bridge module	CAS300M17BM2
Primary to secondary transformer ratio	10:10
Total inductance (µH)	36
DC link capacitance (µF)	200

6.2 Simulation Results

The voltage-current controller of the DAB converter has been implemented in simulation at 40kHz switching frequency. The DC voltage reference tracking has been tested by changing the reference command from 550 to 750V, its efficiency and primary-secondary MOSFETs gate signals, primary-secondary transformer voltages, and inductor current are shown in Fig. 6 (a), (b), and (c) respectively. The DC current reference tracking has been tested by changing the reference command from 20 to 60A, its efficiency and primary-secondary MOSFETs gate signals, primary-secondary transformer voltages, and inductor current are shown in Fig. 7 (a), (b), and (c) respectively. Both controllers i.e., constant voltage and constant control, are practically observed to track the reference signal successfully.

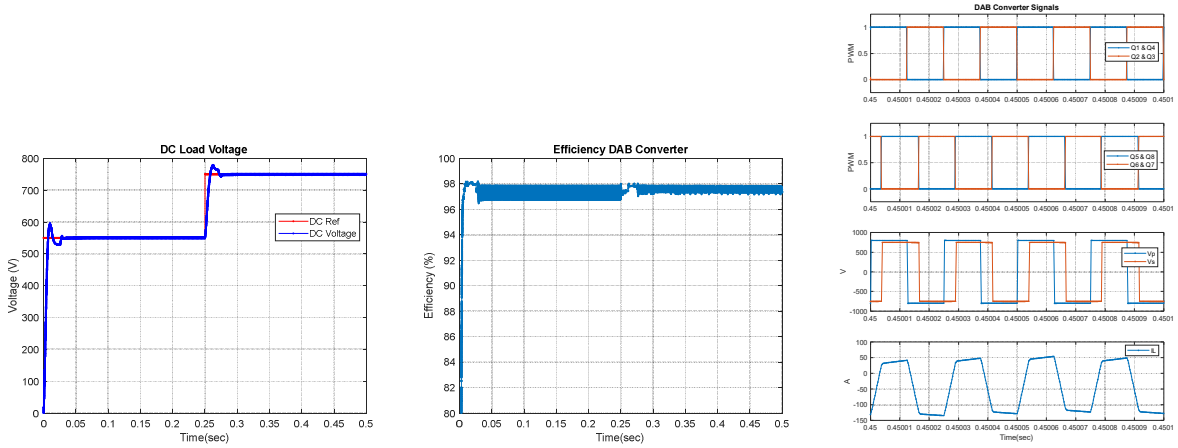

(a) (b) (c)

Fig 6. Constant voltage control: (a) DC voltage tracking, (b) efficiency of DAB converter, c) PWM Signals, transformer primary-secondary voltages and inductor current.

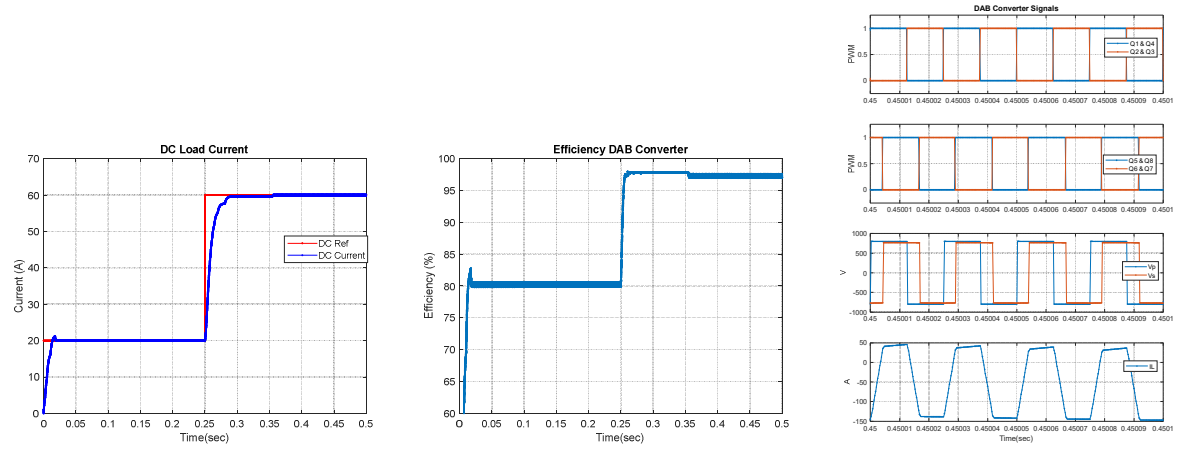

(a) (b) (c)

Fig 7. Constant current control: (a) DC current tracking, (b) efficiency of DAB converter, (c) PWM Signals, transformer primary-secondary voltages and inductor current.

7. Conclusions

In this paper, a 50kW SiC technology-based isolated DAB converter is designed for off-board charging stations. The work is carried out to develop a dynamic simulation model and loss model to estimate the power loss and efficiency of the DAB converter. MATLAB System Identification tool is used to create linear models of DAB converters to perform static stability, controllability analysis and offline control

system design. The proposed CC-CV control strategy is implemented in simulation at a 40kHz switching frequency to charge the batteries at different modes. The closed loop dynamic simulation model is executed to estimate power losses and efficiency accurately. The efficiency of the 50kW three-phase low-frequency transformer (DTF50) is 97%, and its weight is 230kg, which is mentioned in the datasheet. While the total efficiency of the DAB converter is 97.5%, and the estimated weight is about 20kg. It includes power electronics modules, a high-frequency transformer, liquid cooling plate, passive components, gate drivers, PCBs, etc. The estimated parameters depict that the isolated DAB converter has an advantage over low-frequency transformers because of its higher efficiency and less weight. The provided results of controllers prove a correct operation of the entire control system and thus enable an isolated DAB converter for BEVs used in electric vehicle chargers.

Acknowledgements
The authors are grateful to VLAIO (ex. IWT) and Flux50, national funding schemes in Belgium, for the support to the current work, performed within the BELLA project (project ID: HBC.2021.0800). We also acknowledge Flanders Make for the support to our research group.

References

[1] N. S. Pearre and H. Ribberink, "Review of research on V2X technologies, strategies, and operations," *Renewable and Sustainable Energy Reviews*, vol. 105. Elsevier Ltd, pp. 61–70, May 2019, doi: 10.1016/j.rser.2019.01.047.

[2] S. Schey, "Electric vehicle charging infrastructure deployment guidelines British Columbia," 2009.

[3] E. Langer, "Liquid Cooling for EV Charging—What to Know to Keep Electric Vehicles on the Go."

[4] S. Habib, M. M. Khan, F. Abbas, and H. Tang, "Assessment of electric vehicles concerning impacts, charging infrastructure with unidirectional and bidirectional chargers, and power flow comparisons," *Int. J. Energy Res.*, vol. 42, no. 11, pp. 3416–3441, 2018.

[5] T. Braunl, "EV charging standards," *Univ. West. Aust. Perth, Aust.*, pp. 1–5, 2012.

[6] M. Brenna, F. Foiadelli, C. Leone, and M. Longo, "Electric Vehicles Charging Technology Review and Optimal Size Estimation," *J. Electr. Eng. Technol.*, pp. 1–14, 2020.

[7] H. Ramakrishnan, "Bi-Directional dual active bridge reference design for level 3 electric vehicle charging stations," *Syst. Eng. Texas Instruments, India*, 2019.

[8] A. Kulkarni, "Design of Gallium Nitride Transistor Based Dual Active Bridge DC-DC Converter," 2021.

[9] V. Monteiro *et al.*, "Assessment of a battery charger for electric vehicles with reactive power control," in *IECON 2012-38th Annual Conference on IEEE Industrial Electronics Society*, 2012, pp. 5142–5147.

[10] H. Rasool *et al.*, "Design Optimization and Electro-thermal Modelling of an Off-Board Charging System for Electric Bus Applications," *IEEE Access*, 2021.

[11] H. Rasool, A. Zhaksylyk, S. Chakraborty, M. El Baghdadi, and O. Hegazy, "Optimal Design Strategy and Electro-Thermal Modelling of a High-Power Off-Board Charger for Electric Vehicle Applications," in *2020 Fifteenth International Conference on Ecological Vehicles and Renewable Energies (EVER)*, 2020, pp. 1–8.

[12] H. Rasool, M. El Baghdadi, A. M. Rauf, A. Zhaksylyk, and O. Hegazy, "A Rapid Non-Linear Computation Model of Power Loss and Electro Thermal Behaviour of Three-Phase Inverters in EV Drivetrains," in *2020 International Symposium on Power Electronics, Electrical Drives, Automation and Motion (SPEEDAM)*, 2020, pp. 317–323.

[13] D. Graovac, M. Purschel, and A. Kiep, "MOSFET power losses calculation using the data-sheet parameters," *Infineon Appl. note*, vol. 1, pp. 1–23, 2006.

[14] U. Nicolai and A. Wintrich, "Determining switching losses of SEMIKRON IGBT modules," *SEMIKRON Appl. Note, AN*, vol. 1403, 2014.

[15] P. Semiconductors, "Application Manual Power Semiconductors."

[16] J. Guo, "Modeling and design of inverters using novel power loss calculation and dc-link current/voltage ripple estimation methods and bus bar analysis." 2017.

[17] R. W. Erickson and D. Maksimovic, *Fundamentals of power electronics*. Springer Science & Business Media, 2007.